The Stannides $EuPd_2Sn_2$, $EuPt_2Sn_2$, $EuAu_2Sn_2$, and $Eu_3Ag_{5.4}Sn_{5.6}$ – Structure and Magnetic Properties

Christian Schwickert, Florian Winter and Rainer Pöttgen

Institut für Anorganische und Analytische Chemie, Universität Münster, Corrensstrasse 30, 48149 Münster, Germany

Reprint requests to R. Pöttgen. E-mail: pottgen@uni-muenster.de

Z. Naturforsch. **2014**, *69b*, 775 – 785 / DOI: 10.5560/ZNB.2014-4098
Received May 6, 2014

The europium stannides EuT_2Sn_2 (T = Pd, Pt, Au) and $Eu_3Ag_{5.4}Sn_{5.6}$ were synthesized by high-frequency melting of the elements in sealed niobium ampoules in a water-cooled sample chamber. All samples were characterized by powder X-ray diffraction. The EuT_2Sn_2 (T = Pd, Pt, Au) stannides crystallize with the $CaBe_2Ge_2$-type structure, space group $P4/nmm$. The structure of $EuPd_2Sn_2$ was refined from single-crystal X-ray diffractometer data: $a = 462.44(8)$, $c = 1045.8(3)$ pm, $wR = 0.0402$, 237 F^2 values and 15 refined variables. The palladium and tin atoms build up a three-dimensional $[Pd_2Sn_2]$ polyanionic network, exclusively with Pd–Sn interactions (261 – 269 pm). The Pd1 and Pd2 atoms have square-pyramidal and tetrahedral tin coordination, respectively. The europium atoms fill large voids within the network. They are coordinated to eight palladium and eight tin atoms. Temperature-dependent magnetic susceptibility studies confirm a stable divalent ground state of the europium atoms. The compounds become ordered antiferromagnetically below 6.3 ($EuPd_2Sn_2$), 6.1 ($EuPt_2Sn_2$) and 7.7 K ($EuAu_2Sn_2$). $Eu_3Ag_{5.4}Sn_{5.6}$ adopts a partially ordered variant of the La_3Al_{11} type, space group $Immm$, $a = 471.33(8)$, $b = 1382.5(4)$, $c = 1032.4(2)$ pm, $wR = 0.0449$, 692 F^2 values, 30 variables. The three-dimensional $[Ag_{5.4}Sn_{5.6}]$ network shows one silver and one tin site besides two sites with substantial Ag/Sn mixing. The two crystallographically independent europium atoms fill larger and smaller cavities within the $[Ag_{5.4}Sn_{5.6}]$ network. $Eu_3Ag_{5.4}Sn_{5.6}$ also shows divalent europium and antiferromagnetic ordering at $T_N = 6.9$ K. A ^{151}Eu Mössbauer spectrum of $Eu_3Ag_{5.4}Sn_{5.6}$ at 5.2 K shows an isomer shift of $\delta = -10.61$ mm s^{-1}, typical for Eu(II) compounds, and a magnetic hyperfine field splitting of $B_{Hf} = 5.9$ T. ^{119}Sn Mössbauer spectra of the four stannides show isomer shifts in the range of $\delta = 1.78 - 2.20$ mm s^{-1}, usually observed for tin in intermetallic compounds.

Key words: Europium, Stannides, Magnetic Properties, ^{119}Sn Mössbauer Spectroscopy, ^{151}Eu Mössbauer Spectroscopy

Introduction

Ternary rare earth (*RE*) transition metal (*T*) stannides $RE_xT_ySn_z$ have intensively been studied with respect to crystal chemistry and physical properties. Overviews are given in [1, 2]. Such stannides are mostly accessible directly *via* arc-melting of the elements. Exceptions are those based on europium and ytterbium. Synthesis in a quasi-open arc-melting chamber leads to significant europium and ytterbium evaporation since both rare earths have low boiling temperatures, *i. e.* 1870 K for europium and 1466 K for ytterbium [3]. To give an example, for the synthesis of $EuIrSn_2$ [4] and EuPtSn [5], europium starts to boil before iridium (2863 K) and platinum (2045 K) are melted. The evaporation falsifies the composition of the sample, and it is almost impossible to get phase-pure samples on a microscopic scale. Often additions of up to 5 weight-% europium or ytterbium are used in order to compensate for the mass loss and to achieve the desired composition. Even this technique does not improve sample quality. Impurity phases might accumulate at the grain boundaries, and physical property measurements might be affected. Frequently, the experimental magnetic moments of divalent europium and trivalent ytterbium compounds deviate signifi-

		$Eu_2Ni_{2-x}Sn_5$[11]	$Eu_3Cu_8Sn_4$[19] $EuCu_2Sn_2$[17, 20] $EuCuSn_2$[21] $EuCu_9Sn_4$[21] $EuCu_4Sn_2$[21] EuCuSn[22]	EuZnSn[27-29] LT-$EuZn_2Sn_2$[30] HT-$EuZn_2Sn_2$[30]
$EuRuSn_3$[6]	$Eu_3Rh_4Sn_{13}$[7-9]	EuPdSn[5, 12-14] $Eu_3Pd_2Sn_2$[15] $EuPd_2Sn_2$[16, 17]	EuAgSn[18, 22-24] $Eu_3Ag_{5.4}Sn_{5.6}$	EuCdSn[27]
	$EuIrSn_2$[4] $Eu_3Ir_4Sn_{13}$[10]	EuPtSn[5, 13] $Eu_2Pt_3Sn_5$[18] $EuPt_2Sn_2$[17]	EuAuSn[25] $Eu_2Au_2Sn_5$[26] $EuAu_2Sn_2$[16]	

Fig. 1. Structurally characterized europium transition-metal stannides.

cantly from the free ion values. To overcome these evaporation problems, sealed high-melting metal tubes (niobium or tantalum) are the best technique for the preparation of such intermetallics.

Due to the preparative problems, only few europium-based stannides have been reported [4 – 30]. An overview on the existing phases is given in Fig. 1. Most of these stannides contain stable divalent europium, while mixed europium valence has been observed for $EuRuSn_3$ [6]. In continuation of our systematic studies of structure-property relationships of europium-based intermetallics with $ThCr_2Si_2$, $CaBe_2Ge_2$, or related structures, *e. g.* $EuNi_2Sb_2$ [31], $EuGa_2Sb_2$ [32], $EuCd_2Sb_2$ [33], or $EuAu_2Ge_2$ [34], we were interested in the respective stannides. So far, only some conference reports on EuT_2Sn_2 (T = Cu, Pd, Pt, Au) [16, 17] are available in the literature. All these investigations were based on powder X-ray diffraction data. Monoclinic distortions were reported for $EuCu_2Sn_2$, $EuPd_2Sn_2$, and $EuPt_2Sn_2$ [16, 17] and confirmed for $EuCu_2Sn_2$ by a Rietveld refinement [20]. ^{151}Eu Mössbauer spectroscopic data of $EuPd_2Sn_2$ and $EuPt_2Sn_2$ pointed to divalent europium. $EuZn_2Sn_2$ is dimorphic with a $CaBe_2Ge_2$-type high-temperature modification which transforms to a monoclinic low-temperature variant below 645 °C [30]. Europium is divalent in both modifications.

Herein we report on single-crystal X-ray diffraction data of undistorted $EuPd_2Sn_2$ and a detailed study of the magnetic properties of EuT_2Sn_2 with T = Pd, Pt, Au. Phase analytical work in the Eu-Ag-Sn system led to the new stannide $EuAg_{5.4}Sn_{5.6}$ with a partially ordered La_3Al_{11} structure.

Experimental

Synthesis

For a targeted synthesis of EuT_2Sn_2 (T = Pd, Pt, Au) and $Eu_3Ag_{5.4}Sn_{5.6}$, europium pieces (Smart Elements, > 99.9 %), a palladium plate (Allgussa AG, 99.9 %), platinum sponge (Degussa Hüls, 99.9 %), silver ingots (Allgussa AG, 99.9 %), pieces of a gold bar (Allgussa AG, 99.9 %), and tin granules (Merck, > 99.99 %) were used. Suitable europium pieces were mechanically cleaned from surface impurities and arc-melted [35] to small compact buttons which were stored in Schlenk tubes under argon atmosphere prior to the reactions. The argon was purified over titanium sponge (900 K), silica gel, and molecular sieves.

Mixtures with stoichiometric ratios of the educts were arc-welded into niobium ampoules under an argon atmosphere of *ca.* 700 mbar. The ampoules were then placed in a water-cooled sample chamber of an induction furnace [36] (Typ TIG 2.5/300, Hüttinger Elektronik, Freiburg, Germany) and rapidly heated to *ca.* 1500 K. After 15 min the temperature was slowly reduced to 1100 K within another 15 min. Subsequently the samples were annealed at that temperature for another four hours before quenching the reaction mixture by turning off the high-frequency generator. The resulting ingots are fairly brittle and exhibit silvery luster, while ground powders appear light grey. No reaction with the container material was evident, and the resulting compounds are stable in air over months.

EDX data

Semiquantitative EDX analyses of the $EuPd_2Sn_2$ and $Eu_3Ag_{5.4}Sn_{5.6}$ single crystals studied on the diffractometer were carried out in variable pressure mode with a Zeiss EVO® MA10 scanning electron microscope with EuF_2, Pd,

Compound	a (pm)	b (pm)	c (pm)	β (deg)	V (nm^3)	Reference
$EuPd_2Sn_2$	462.44(8)	a	1045.8(3)	90	0.2236	this work
$EuPd_2Sn_2$	465.2	463.1	1042.5	90.83	0.2246	[16]
$EuPd_2Sn_2$	465.20(3)	463.10(3)	1042.50(7)	90.83(6)	0.2246	[17]
$EuPt_2Sn_2$	462.39(5)	a	1024.0(2)	90	0.2189	this work
$EuPt_2Sn_2$	464.61(3)	464.45(3)	1035.29(6)	92.32(1)	0.2232	[17]
$EuAu_2Sn_2$	463.32(7)	a	1123.9(3)	90	0.2413	this work
$EuAu_2Sn_2$	462.1	a	1122.8	90	0.2398	[16]
$Eu_3Ag_{5.4}Sn_{5.6}$	471.33(8)	1382.5(4)	1032.4(2)	90	0.6727	this work

Table 1. Lattice parameters (Guinier technique) of the stannides EuT_2Sn_2 (T = Pd, Pt, Au), space group $P4/nmm$, and $Eu_3Ag_{5.4}Sn_{5.6}$, space group $Immm$.

Ag, and Sn as standards. The experimentally observed average compositions (21 ± 1 at.-% Eu : 39 ± 1 at.-% Pd : 40 ± 1 at.-% Sn and 20 ± 2 at.-% Eu : 37 ± 2 at.-% Ag : 43 ± 2 at.-% Sn) were close to the ideal ones, and no impurity elements heavier than boron (detection limit of the instrument) were detected. The standard deviations account for the variations in the point analyses on various parts of the irregularly-shaped (conchoidal fracture) crystals.

X-Ray diffraction

The polycrystalline EuT_2Sn_2 (T = Pd, Pt, Au) and $Eu_3Ag_{5.4}Sn_{5.6}$ samples were studied by powder X-ray diffraction using the Guinier technique: imaging plate detector (Fujifilm BAS-1800), CuK_{α_1} radiation and α-quartz ($a = 491.30$, $c = 540.46$ pm) as an internal standard. The lattice parameters (Table 1) were obtained from least-squares refinements. Correct indexing was ensured through intensity calculations [37]. The single-crystal and powder lattice parameters of $EuPd_2Sn_2$ and $Eu_3Ag_{5.4}Sn_{5.6}$ agreed well (Table 2).

Irregularly shaped single-crystal fragments of $EuPd_2Sn_2$ and $Eu_3Ag_{5.4}Sn_{5.6}$ were selected from the bulk samples by mechanical separation. The crystallites were glued to tiny quartz fibers using beeswax, and their quality was checked on a Buerger camera (using white Mo radiation). The intensity data collection was performed on a Stoe IPDS-II image plate system (graphite-monochromatized MoK_α radiation; $\lambda = 71.073$ pm) in oscillation mode. Both data sets were subjected to a numerical absorption correction. Details of the data collections and the crystallographic parameters are listed in Table 2.

Structure refinements

Isotypy of $EuPd_2Sn_2$ with the $CaBe_2Ge_2$-type structure [38] was already evident from the Guinier powder pattern. The systematic extinctions were compatible with space group $P4/nmm$, and the standardized positional parameters of the prototype [39] were taken as starting values. The $Eu_3Ag_{5.4}Sn_{5.6}$ intensity data set showed an I-centered orthorhombic lattice and no additional systematic extinctions. The centrosymmetric space group $Immm$ was found to be correct during structure refinement. The starting atomic parameters of $Eu_3Ag_{5.4}Sn_{5.6}$ were obtained by the charge-flipping algorithm of SUPERFLIP [40]. Both structures were then refined on F^2 with anisotropic displacement parameters for all atoms with JANA2006 [41]. In order to check for the correct compositions, the occupancy parameters of both crystals were refined in a separate series of least-squares cycles. In the case of $EuPd_2Sn_2$ all sites were fully occupied within three standard deviations while one Ag and one Sn site in the structure of $Eu_3Ag_{5.4}Sn_{5.6}$ showed higher, respectively lower scattering power. The Ag/Sn mixings for these sites were then refined as a least-squares variable in the final cycles. The final difference Fourier syntheses revealed no significant residual peaks. The final positional parameters and interatomic distances are listed in Table 3 – 5.

Table 2. Crystal data and structure refinement for $EuPd_2Sn_2$ and $Eu_3Ag_{5.4}Sn_{5.6}$.

Empirical formula	$EuPd_2Sn_2$	$Eu_3Ag_{5.4}Sn_{5.6}$
Formula weight, g mol^{-1}	602.2	1703.0
Unit cell dimensions	Table 1	Table 1
Space group, Z	$P4/nmm$, 2	$Immm$, 2
Calculated density, g cm^{-3}	8.94	8.40
Crystal size, μm^3	$10 \times 50 \times 60$	$20 \times 20 \times 100$
Transmission ratio (min/max)	0.161/0.443	0.170/0.358
Absorption coefficient, mm^{-1}	32.5	31.5
F(000), e	510	1445
θ range for data collection, deg	4–35	2–32
Range in hkl	±7, ±7, ±16	±7, ±20, ±15
Total no. of reflections	15 560	12 030
Independent reflections/R_{int}	237/0.0535	692/0.0916
Reflections with $I > 3\,\sigma(I)/R_\sigma$	209/0.0030	642/0.0048
Data/parameters	237/15	692/30
Goodness-of-fit on F^2	1.45	1.74
R/wR for $I > 3\,\sigma(I)$	0.0164/0.0392	0.0192/0.0442
R/wR for all data	0.0193/0.0402	0.0219/0.0449
Extinction coefficient	1280(90)	2080(100)
Largest diff. peak/hole, e Å^{-3}	1.11/−1.27	1.11/−1.37

Further details of the crystal structure investigation may be obtained from Fachinformationszentrum Karlsruhe, 76344 Eggenstein-Leopoldshafen, Germany (fax: +49-7247-808-666; e-mail: crysdata@fiz-karlsruhe.de, http://www.fiz-karlsruhe.de/request_for_deposited_data.html) on quoting

Table 3. Atomic coordinates and equivalent, isotropic displacement parameters (pm^2) for $EuPd_2Sn_2$ and $Eu_3Ag_{5.4}Sn_{5.6}$. U_{eq} is defined as one third of the trace of the orthogonalized U_{ij} tensor.

Atom	Site	x	y	z	U_{eq}
$EuPd_2Sn_2$					
Eu	2*c*	1/4	1/4	0.75440(3)	163(1)
Pd1	2*c*	1/4	1/4	0.36779(6)	195(1)
Pd2	2*a*	3/4	1/4	0	298(1)
Sn1	2*b*	3/4	1/4	1/2	154(1)
Sn2	2*c*	1/4	1/4	0.11864(7)	295(1)
$Eu_3Ag_{5.4}Sn_{5.6}$					
Eu1	2*a*	0	0	0	128(1)
Eu2	4*g*	0	0.30325(2)	0	112(1)
Ag1	4*j*	0	1/2	0.18949(6)	203(2)
Sn1	2*c*	0	0	1/2	169(2)
50(4) % Ag2	8*l*	0	0.13798(3)	0.27860(4)	162(1)
50(4) % Sn2					
36(3) % Ag3	8*l*	0	0.34077(3)	0.36429(4)	150(1)
64(3) % Sn3					

the deposition number CSD-427712 ($EuPd_2Sn_2$) and CSD-427713 ($Eu_3Ag_{5.4}Sn_{5.6}$).

Magnetic susceptibility studies

The physical property measurements of all compounds were carried out on a Quantum Design physical property measurement system (PPMS) using the VSM and heat capacity options. For the measurements with the VSM option, ground powders of each sample were packed inside a polypropylene capsule and attached to a sample holder rod. The measurements were performed in the temperature range of 3 – 305 K with magnetic flux densities up to 80 kOe ($1\ kOe = 7.96 \times 10^4\ A\,m^{-1}$). For the heat capacity measurement a suitable amount of $Eu_3Ag_{5.4}Sn_{5.6}$ was pressed into a pellet and attached to a standard QD heat capacity puk with ApiezonN grease. The measurement was carried out without an external field in the temperature range of 2 – 305 K.

Table 4. Interatomic distances (pm) for $EuPd_2Sn_2$, calculated with the powder lattice parameters. Standard deviations are equal to or smaller than 0.2 pm. All distances of the first coordination spheres are listed.

Eu:	4	Pd2	345.6	Pd2:	4	Sn2	262.4
	4	Pd1	351.1		4	Pd2	327.0
	4	Sn1	352.5		4	Eu	345.6
	4	Sn2	352.9	Sn1:	4	Pd1	269.4
Pd1:	1	Sn2	260.6		4	Sn1	327.0
	4	Sn1	269.4		4	Eu	352.5
	4	Eu	351.1	Sn2:	1	Pd1	260.6
					4	Pd2	262.4
					4	Eu	352.9

^{119}Sn and ^{151}Eu Mössbauer spectroscopy

$Ca^{119m}SnO_3$ and $^{151}Sm{:}EuF_3$ sources were used for the Mössbauer spectroscopic experiments. The measurements were carried out in a liquid nitrogen cryostat at 78 K and in a liquid helium cryostat at 78 and 5.2 K. The Mössbauer sources were kept at room temperature. The samples were enclosed in small PMMA containers with a mass of 100 mg of the stannides. A palladium foil of 0.05 mm thickness was used to reduce Sn*K* X-rays concurrently emitted by this source. Fitting of the spectra was performed with the NORMOS-90 program system [42].

Discussion

Crystal chemistry

So far, only the structures of $EuCu_2Sn_2$ [20] and $EuZn_2Sn_2$ [30] have been refined from single-crystal diffractometer data. All other studies rely on powder diffraction data. The single-crystal data clearly confirmed the substantial monoclinic distortion for the copper and the dimorphism for the zinc com-

Table 5. Interatomic distances (pm) for $Eu_3Ag_{5.4}Sn_{5.6}$, calculated with the powder lattice parameters. Standard deviations are equal to or smaller than 0.2 pm. All distances of the first coordination spheres are listed. Note the mixed occupancies listed in Table 3.

Eu1:	4	Ag2/Sn2	345.1	Ag1:	2	Sn3/Ag3	284.7	Ag2/	2	Sn3/Ag3	279.6	Sn3/ 2 Ag2/Sn2 279.6
	8	Sn3/Ag3	351.6		4	Ag2/Sn2	305.0	Sn2:	1	Sn3/Ag3	294.0	Ag3: 1 Sn3/Ag3 280.2
	4	Ag1	397.9		2	Sn1	306.3		1	Sn1	297.7	1 Ag1 284.7
	2	Eu2	419.3		2	Eu2	335.1		2	Ag1	305.0	1 Ag2/Sn2 294.0
Eu2:	2	Ag1	335.1		1	Ag1	391.3		2	Eu2	338.2	2 Eu2 338.8
	4	Ag2/Sn2	338.2		2	Eu1	397.9		1	Eu1	345.1	2 Eu1 351.6
	4	Sn3/Ag3	338.8	Sn1:	4	Ag2/Sn2	297.7		1	Eu2	367.3	1 Eu2 379.7
	2	Sn1	359.9		4	Ag1	306.3		1	Ag2/Sn2	381.5	2 Sn3/Ag3 417.4
	2	Ag2/Sn2	367.2		4	Eu2	359.9					
	2	Sn3/Ag3	379.7									
	1	Eu1	419.3									

pound. Although powder diffraction data with monoclinic distortions were reported also for $EuPd_2Sn_2$ and $EuPt_2Sn_2$ [16, 17], our single-crystal data on $EuPd_2Sn_2$ clearly support the tetragonal $CaBe_2Ge_2$-type structure. Our Guinier patterns of $EuPt_2Sn_2$ and $EuAu_2Sn_2$ showed isotypism with $EuPd_2Sn_2$ and no splitting of reflections as a consequence of a monoclinic distortion.

The unit cell of $EuPd_2Sn_2$ is presented in Fig. 2. The structure comprises one europium, two palladium, and two tin sites. The Pd2 and Sn1 atoms both have tetrahedral coordination, *i. e.* Pd2@$Sn2_4$ and Sn1@$Pd1_4$. These tetrahedra share common edges, leading to layers at $z = 0$ and $z = 1/2$ which are separated and charge-balanced by the europium atoms. The layers are connected by Pd–Sn bonds. Within the three-dimensional $[Pd_2Sn_2]$ network the Pd–Sn distances cover the small range from 261 to 269 pm, close to the sum of the covalent radii for Pd + Sn of 268 pm [3]. In the binary palladium stannides $PdSn_2$, $PdSn_3$ and $PdSn_4$ the Pd–Sn distances in the square antiprisms are slightly longer (278 – 284 pm) [43]. We can thus assume strong covalent Pd–Sn bonding within the $[Pd_2Sn_2]$ network. Each europium atom has four nearest palladium neighbors at Eu–Pd distances of 346 and 351 pm. This Eu–Pd bonding is expected from the standard electronegativities.

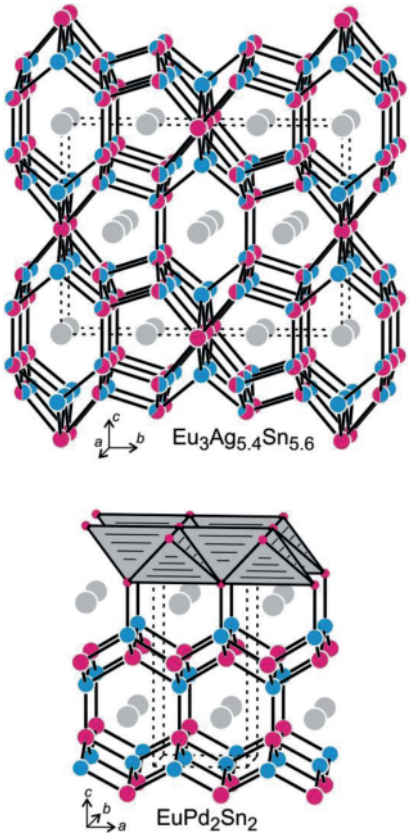

Fig. 2 (color online). The crystal structures of $Eu_3Ag_{5.4}Sn_{5.6}$ (partially ordered La_3Al_{11} type, *Immm*) and $EuPd_2Sn_2$ ($CaBe_2Ge_2$ type, $P4/nmm$). Europium, silver (palladium) and tin atoms are drawn as medium grey, blue and red circles, respectively. The three-dimensional $[Ag_{5.4}Sn_{5.6}]$ and $[Pd_2Sn_2]$ polyanionic networks and one layer of edge-sharing $PdSn_{4/4}$ tetrahedra of $EuPd_2Sn_2$ are emphasized. The mixed-occupied Ag/Sn sites of $Eu_3Ag_{5.4}Sn_{5.6}$ are emphasized by segments.

The Pd2–Pd2 and Sn1–Sn1 distances within the square grids are at 327 pm. For the Pd–Pd contacts one can assume at least weak bonding character. This is also evident from electronic structure calculations on structurally closely related pnictides [44]. The Sn–Sn distances are only slightly longer than in β-Sn (4×302 and 2×318 pm) [45], and we can ascribe weak Sn–Sn bonding.

The structure of $Eu_3Ag_{5.4}Sn_{5.6}$ shows some similarities with that of $EuPd_2Sn_2$, but it is more complex. The europium substructure consists of three body-centered tetragonal subcells which are condensed in *b* direction. These europium subcells are similar to those of the $CaBe_2Ge_2$-type stannides discussed above. The significant difference concerns the polyanionic network. One of the transition metal-tin pairs of the subcell structure is reduced to a single site. This peculiar arrangement has first been observed for the binary aluminide La_3Al_{11} [46], and a fully ordered version occurs in $Dy_3Co_6Sn_5$ [47].

For the $Eu_3Ag_{5.4}Sn_{5.6}$ crystal only the $4j$ and $2c$ sites show full occupancy with silver and tin, respectively, while both $8l$ sites show substantial silver-tin mixing (Table 3). As a consequence of the mixed occupancies, within the three-dimensional $[Ag_{5.4}Sn_{5.6}]$ network we can only discuss the range of the Ag/Sn–Ag/Sn distances, *i. e.* 280 – 306 pm. The shorter ones compare well with the sum of the covalent radii for Ag + Sn of 274 pm [3]. Similar Ag–Sn distances occur in related rare earth-based stannides, *e. g.* ScAgSn (273 – 280 pm) [48] or YbAgSn (277 – 280 pm) [49]. Keeping the Sn–Sn distances of β-Sn (*vide supra*) and *fcc* silver (289 pm) [45] in mind, it is clear that the $[Ag_{5.4}Sn_{5.6}]$ network is stabilized by Ag–Sn, Ag–Ag and Sn–Sn bonding.

The different topology of the $[Ag_{5.4}Sn_{5.6}]$ network (as compared to the EuT_2Sn_2 stannides discussed above) results in two different types of cavities filled by the Eu1 and Eu2 atoms (Fig. 2). Both europium sites have coordination number 16, however, with different ranges for the interatomic distances. For Eu1 the coordination should be called 12 + 4, since the four silver atoms are at relatively long Eu1–Ag distances of 398 pm. In contrast, all sixteen neighbors of the Eu2 atoms are at distances below 380 pm. Although we observe these severe differences in the distance ranges, both crystallographically independent europium sites in $Eu_3Ag_{5.4}Sn_{5.6}$ are in a stable divalent oxidation state (*vide infra*).

Finally we draw back to the non-integer composition of $Eu_3Ag_{5.4}Sn_{5.6}$. Given the fully ordered structure of $Dy_3Co_6Sn_5$ [47], one would expect complete silver-tin ordering. Nevertheless, we observe mixed occupancy for the two 8*l* sites, similar to the equiatomic stannide EuAgSn [22]. Ordered occupancies for La_3Al_{11} derivatives have been observed for composition 3-6-5, 3-7-4, and 3-8-3. These phases crystallize with site occupancy variants/subgroups of La_3Al_{11}. The corresponding group-subgroup schemes have recently been summarized [50].

Magnetic properties

The magnetic property data of EuT_2Sn_2 (T = Pd, Pt, Au) and $Eu_3Ag_{5.4}Sn_{5.6}$ are listed in Table 6. Figs. 3 – 6 (top) show the temperature dependence of the magnetic and inverse magnetic susceptibilities (χ and χ^{-1} data) of the respective compounds in the temperature range 3 – 300 K with an applied field of 10 kOe. In all four measurements an anomaly is evident, and therefore additional measurements with low field strengths (100 Oe) have been conducted (Figs. 3 – 6 top: insets). In all cases antiferromagnetic ordering was observed below 10 K (*cf.* Table 6). Fits of the inverse magnetic susceptibility data with the Curie-Weiss law led to the parameters listed in Table 6. The experimental magnetic moments (μ_{eff}) of the EuT_2Sn_2 compounds compare well with the theoretical value of μ_{eff} = 7.94 μ_B per Eu^{2+} ion while it is slightly lower for $Eu_3Ag_{5.4}Sn_{5.6}$. The Weiss constants θ_P are indicative of antiferromagnetic interactions in the paramagnetic domain for the gold and silver compounds, while the other two exhibit slightly positive values that are a sign of weak ferromagnetic interactions in the paramagnetic

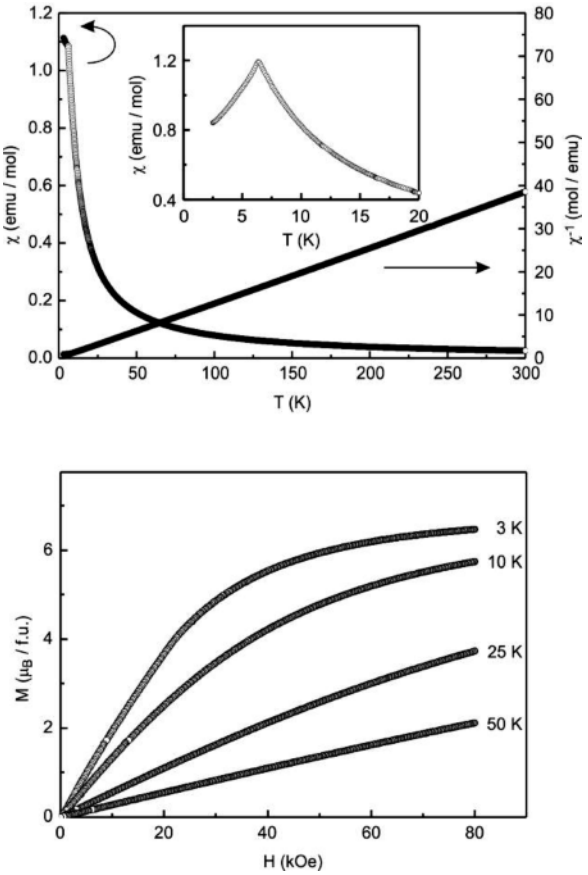

Fig. 3. Temperature dependence of the magnetic and inverse magnetic susceptibility data (χ and χ^{-1}) of $EuPd_2Sn_2$ with an applied field of 10 kOe (top). The inset puts emphasis on the low-temperature region of a low-field measurement (H = 100 Oe). Magnetization isotherms of $EuPd_2Sn_2$ taken at 3, 10, 25, and 50 K with an applied field of up to 80 kOe (bottom).

domain. In the case of $EuAu_2Sn_2$ the low field measurement in zero-field-cooled (ZFC)/field-cooled (FC) mode there is some bifurcation evident below 25 K. This has to be attributed to an unknown ferromagnetic impurity.

In addition, magnetization isotherms were recorded at various temperatures (Figs. 3 – 5 bottom; Fig. 6 center). It is noteworthy that while the 3 K isotherms of $EuPd_2Sn_2$ and $EuPt_2Sn_2$ have the course of a typical antiferromagnet the magnetization isotherm of $EuAu_2Sn_2$ at 3 K increases almost linearly with the applied field as is typical for a paramagnetic material. It does show a minute *s*-like curvature and ex-

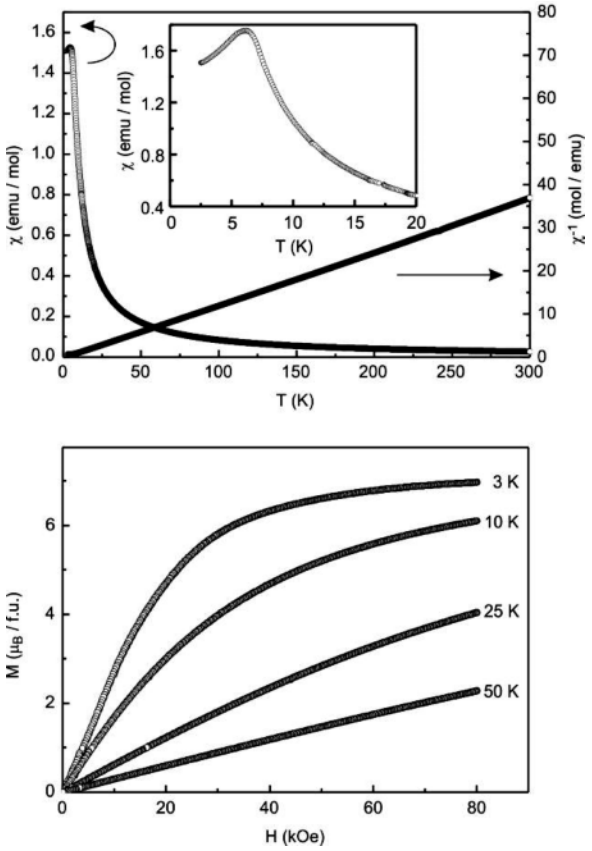

Fig. 4. Temperature dependence of the magnetic and inverse magnetic susceptibility data (χ and χ^{-1}) of $EuPt_2Sn_2$ with an applied field of 10 kOe (top). The inset emphasizes the low-temperature region of a low-field measurement ($H = 100$ Oe). Magnetization isotherms of $EuPt_2Sn_2$ taken at 3, 10, 25, and 50 K with an applied field of up to 80 kOe (bottom).

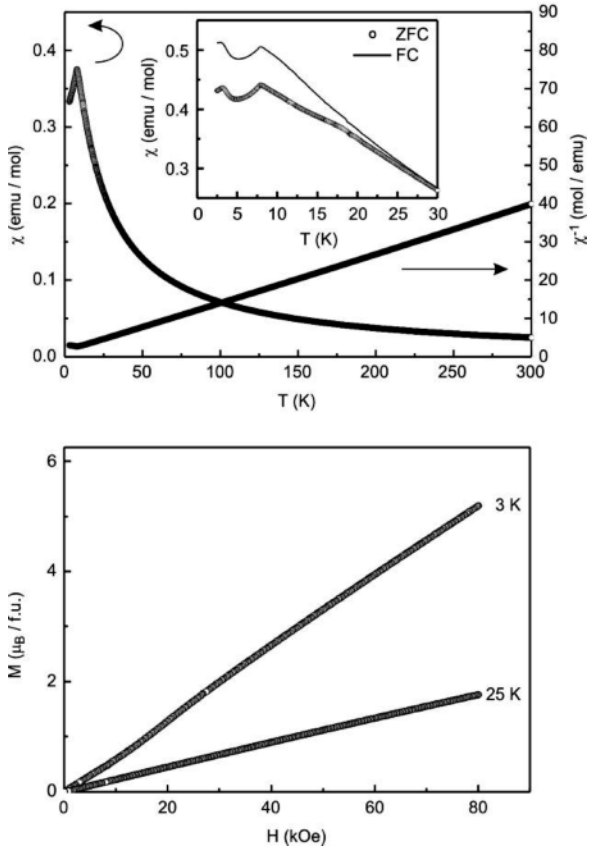

Fig. 5. Temperature dependence of the magnetic and inverse magnetic susceptibility data (χ and χ^{-1}) of $EuAu_2Sn_2$ with an applied field of 10 kOe (top). The inset shows the low-temperature region of a low-field measurement ($H = 100$ Oe) in zero-field-cooled (ZFC)/field-cooled (FC) mode. Magnetization isotherms of $EuAu_2Sn_2$ taken at 3 and 25 K with an applied field of up to 80 kOe (bottom).

hibits a weak metamagnetic step at a critical field $H_C = 15$ kOe confirming an antiferromagnetic ground state. In the case of $Eu_3Ag_{5.4}Sn_{5.6}$ the low-field measurement in ZFC/FC mode revealed a second anomaly at 3.4 K. Therefore magnetization isotherms were measured at 2.5, 5, 10, 25, and 50 K in order to resolve the two phenomena. The isotherms in general show weak curvature, and the isotherm at 2.5 K (Fig. 6 bottom: red curve) exhibits a metamagnetic step at a critical field strengths of $H_C = 20$ kOe, so an antiferromagnetic ground state can be assumed as well. The magnetization isotherm at 5 K, thus in between the two anomalies, does not show any sign of spin reorientation. In order to verify that both anomalies are intrinsic in nature a heat capacity measurement was performed. The corresponding temperature-dependent results are depicted in Fig. 6 (bottom) with an enlargement of the low-temperature range in the inset. The unusually broad peak can be attributed to a superposition of two smaller λ-type peaks as indicated by the local minimum at 5 K. It was possible to ascertain the higher ordering temperature ($T_N = 6.9$ K) obtained from the magnetic measurements. As the two peaks are similar in their intensity, both can be considered intrinsic. The anomaly at room temperature can be attributed to the ApiezonN grease [51] used as contacting agent. Keep-

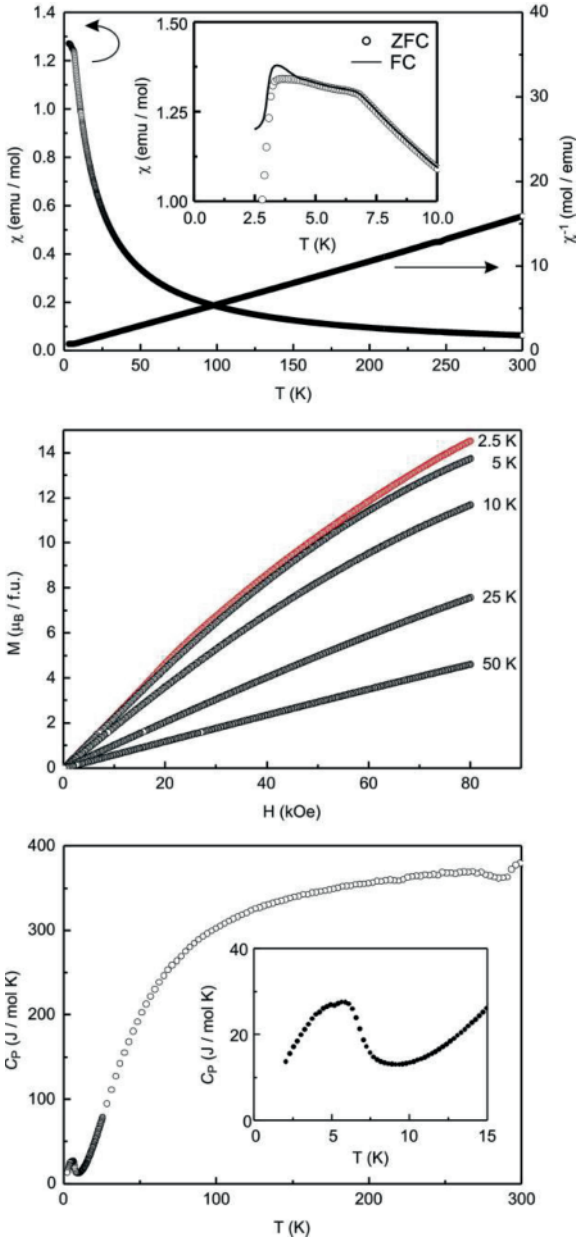

Fig. 6 (color online). Temperature dependence of the magnetic and inverse magnetic susceptibility data (χ and χ^{-1}) of $Eu_3Ag_{5.4}Sn_{5.6}$ with an applied field of 10 kOe (top). The low-temperature region of a low-field measurement at 100 Oe in zero-field-cooled (ZFC)/field-cooled (FC) mode is depicted in the inset. Magnetization isotherms of $Eu_3Ag_{5.4}Sn_{5.6}$ taken at 2.5, 5, 10, 25, and 50 K with an applied field of up to 80 kOe (center). Heat capacity measurement data of $Eu_3Ag_{5.4}Sn_{5.6}$ without external magnetic field (bottom). The inset shows a blow-up of the low-temperature range of the measurement.

ing in mind that there are two crystallographically independent Eu sites in $Eu_3Ag_{5.4}Sn_{5.6}$ with a ratio of 2(Eu2) : 1(Eu1), a possible explanation of the two observed phenomena is that at 6.9 K the spins of both sites align in an antiparallel fashion leading to a ferrimagnetic state as the Eu1–Eu2 distance is the shortest europium distance in the structure. Upon further cooling the spins realign in a way that now both sites show antiferromagnetic ordering leading to an antiferromagnetic ground state below 3.4 K.

Mössbauer spectroscopy

The ^{119}Sn Mössbauer spectra of EuT_2Sn_2 (T = Pd, Pt, Au) and $Eu_3Ag_{5.4}Sn_{5.6}$ recorded at 78 K together with the transmission integral fits are presented in Fig. 7, and their corresponding fitting parameters are listed in Table 7. In accordance with the two crystallographically independent tin sites in EuT_2Sn_2, the spectra could be reproduced by a superposition of two independent signals with isomer shifts δ = 1.78 – 2.20 mm s^{-1}. The assignment of the two signals is feasible through the transition metal coordination of the Sn1 and Sn2 sites. The signals with larger quadrupole splitting (blue) can be assigned to the Sn2 site with square-pyramidal transition metal coordination showing higher asymmetry. In the case of the Pd and Pt compounds the isomer shift of the signals is identical within the standard deviation. In the gold stannide, however, the signal corresponding to Sn2 shows a higher isomer shift, indicating slightly higher s electron density at these nuclei. The ratios of the two signals were refined to the ideal 50 : 50 ratio in the case of $EuAu_2Sn_2$ and kept fixed for the other two compounds showing clearly that there is no site disorder on the T and Sn sites in the bulk samples.

The spectrum of $Eu_3Ag_{5.4}Sn_{5.6}$ was fitted with two independent signals with isomer shifts of δ = 1.83(2) and 2.20(1) mm s^{-1} with a refined ratio of 17(1) : 83(1). The smaller signal corresponds to the Sn1 site and the bigger one to a superposition of the two expected signals for the Ag2/Sn2 and Sn3/Ag3 sites. This superposition is also evident from the enhanced line width. All four spectra exhibit isomer shifts in the range expected for intermetallic stannides [26, 52 – 54].

Fig. 8 shows the ^{151}Eu Mössbauer spectra of $Eu_3Ag_{5.4}Sn_{5.6}$ together with the transmission inte-

Table 6. Magnetic properties of EuT_2Sn_2 (T = Pd, Pt, Au) and $Eu_3Ag_{5.4}Sn_{5.6}$: μ_{exp}, experimental magnetic moment; μ_{eff} = 7.94 μ_B per Eu^{2+}, effective magnetic moment; θ_P, paramagnetic Curie temperature; μ_{sm}, experimental saturation magnetization; $\mu_{sm(calcd)}$, calculated saturation magnetization; T_N, Néel temperature.

Compound	μ_{exp} (μ_B per Eu)	θ_P (K)	μ_{sm} (μ_B per fu)	$\mu_{sm(calcd)}$ (μ_B per fu)	T_N (K)
$EuPd_2Sn_2$	7.89(1)	1.4(5)	6.5(1)	7	6.3(5)
$EuPt_2Sn_2$	8.05(1)	3.4(5)	7.0(1)	7	6.1(5)
$EuAu_2Sn_2$	7.91(1)	−10.1(5)	5.2(1)	7	7.7(5)
$Eu_3Ag_{5.4}Sn_{5.6}$	7.41(1)	−10.4(5)	14.5(1)	21	6.9(5)/3.4(5)

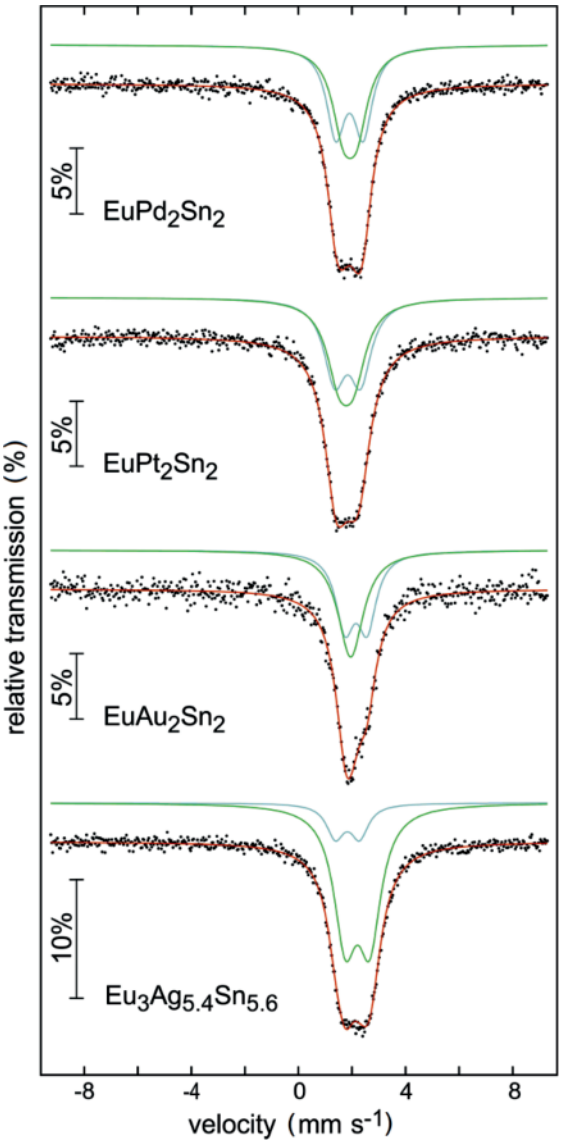

Fig. 7 (color online). Experimental (data points) and simulated (continuous lines) ^{119}Sn Mössbauer spectra of EuT_2Sn_2 (T = Pd, Pt, Au) and $Eu_3Ag_{5.4}Sn_{5.6}$ at 78 K.

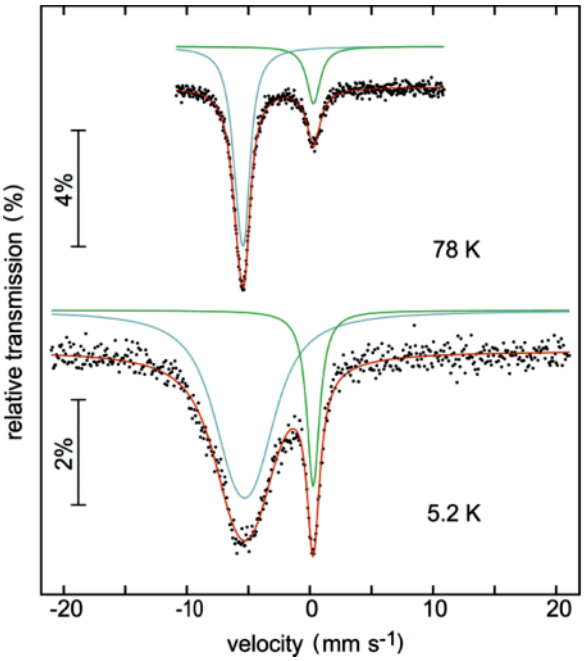

Fig. 8 (color online). Experimental (data points) and simulated (continuous lines) ^{151}Eu Mössbauer spectra of $Eu_3Ag_{5.4}Sn_{5.6}$ at 78 and 5.2 K.

Table 7. Fitting parameters of ^{119}Sn Mössbauer spectroscopic measurements at 78 K of EuT_2Sn_2 (T = Pd, Pt, Au) and $Eu_3Ag_{5.4}Sn_{5.6}$; δ = isomer shift, ΔE_Q = electric quadrupole splitting, Γ = experimental line width.

Compound	Signal	Area (%)	δ (mm s^{-1})	ΔE_Q (mm s^{-1})	Γ (mm s^{-1})
$EuPd_2Sn_2$	1	50[a]	1.90(1)	1.02(2)	0.84(3)
	2	50[a]	1.92(1)	0.50(5)	1.01(5)
$EuPt_2Sn_2$	1	50[a]	1.83(1)	0.97(4)	0.98(6)
	2	50[a]	1.78(1)	0.5(1)	1.1(1)
$EuAu_2Sn_2$	1	50(1)	2.15(2)	0.8(1)	0.8(1)
	2	50(1)	1.95(6)	0[a]	1.2(1)
$Eu_3Ag_{5.4}Sn_{5.6}$	1	17(1)	1.83(2)	0.90(2)	0.80[a]
	2	83(1)	2.20(1)	0.92(1)	1.04(1)

[a] Fixed parameter.

Compound	T (K)	Area (%)	δ (mm s^{-1})	ΔE_Q (mm s^{-1})	Γ (mm s^{-1})	B_{Hf} (T)
$Eu_3Ag_{5.4}Sn_{5.6}$	78	79(1)	−11.06(1)	3.1(1)	2.35(4)	–
Eu_2O_3	78	21(1)	0.60(3)	0[a]	2.63(7)	–
$Eu_3Ag_{5.4}Sn_{5.6}$	5.2	81(1)	−10.61(5)	0[a]	7.9(5)	5.9(5)
Eu_2O_3	5.2	19(1)	0.55(2)	0[a]	2.50(8)	–

[a] Fixed parameter.

Table 8. Fitting parameters of ^{151}Eu Mössbauer spectroscopic measurements at 78 and 5.2 K of $Eu_3Ag_{5.4}Sn_{5.6}$; δ = isomer shift, ΔE_Q = electric quadrupole splitting, Γ = experimental line width, B_{Hf} = magnetic hyperfine splitting.

gral fits (78 and 5.2 K data). The corresponding fitting parameters are listed in Table 8. The observed spectra were fitted with two signals. The one at $\delta = -10.61(5)$ mm s^{-1} (5.2 K) corresponds to the Eu atoms of the sample and exhibits a moderate hyperfine field splitting, due to the fact that the magnetic ordering of the sample is not yet complete at that temperature (*vide supra*). It is thus a superposition of the two expected signals of crystallographically independent Eu sites in $Eu_3Ag_{5.4}Sn_{5.6}$ with similar coordination. The isomer shift is in the typical range of Eu(II) in intermetallic compounds. The second signal can be attributed to Eu_2O_3 (surface oxidation of the compound during grinding) explaining the slightly reduced magnetic moment and the reduction of the maximum magnetization.

Acknowledgement

We thank Dipl.-Ing. U. Ch. Rodewald for the intensity data collections. This work was financially supported by the Deutsche Forschungsgemeinschaft through SPP 1458 *Hochtemperatursupraleitung in Eisenpnictiden*.

[1] R. V. Skolozdra, in *Handbook on the Physics and Chemistry of Rare Earths*, (Eds.: K. A. Gschneidner Jr., L. Eyring), Elsevier Science, Amsterdam, **1997**, chapter 164, pp. 399 – 517.
[2] R. Pöttgen, *Z. Naturforsch.* **2006**, *61b*, 677.
[3] J. Emsley, *The Elements*, Oxford University Press, Oxford **1999**.
[4] R. Pöttgen, R.-D. Hoffmann, M. H. Möller, G. Kotzyba, B. Künnen, C. Rosenhahn, B. D. Mosel, *J. Solid State Chem.* **1999**, *145*, 174.
[5] R. Pöttgen, *Z. Naturforsch.* **1996**, *51b*, 806.
[6] T. Harmening, W. Hermes, M. Eul, R. Pöttgen, *Solid State Sci.* **2010**, *12*, 284.
[7] A. S. Cooper, *Mater. Res. Bull.* **1980**, *15*, 799.
[8] J. L. Hodeau, M. Marezio, J. P. Remeika, C. H. Chen, *Solid State Commun.* **1982**, *42*, 97.
[9] S. Miraglia, J. L. Hodeau, M. Marezio, C. Laviron, M. Ghedira, G. P. Espinosa, *J. Solid State Chem.* **1986**, *63*, 358.
[10] Y. Aoki, T. Fukuhara, H. Sugawara, H. Sato, *J. Phys. Soc. Jpn.* **1996**, *65*, 1005.
[11] T. Harmening, M. Eul, R. Pöttgen, *Z. Naturforsch.* **2009**, *64b*, 1107.
[12] D. T. Adroja, S. K. Malik, *Phys. Rev. B* **1992**, *45*, 779.
[13] R. Müllmann, U. Ernet, B. D. Mosel, H. Eckert, R. K. Kremer, R.-D. Hoffmann, R. Pöttgen, *J. Mater. Chem.* **2001**, *11*, 1133.
[14] P. Lemoine, J. M. Cadogan, D. H. Ryan, M. Giovannini, *J. Phys.: Condens. Matter* **2012**, *24*, 236004.
[15] P. Solokha, I. Čurlik, M. Giovannini, N. R. Lee-Hone, M. Reiffers, D. H. Ryan, A. Saccone, *J. Solid State Chem.* **2011**, *184*, 2498.
[16] Z. Hossain, C. Mazumdar, R. Nagarajan, C. Godart, L. C. Gupta, B. D. Padalia, R. Vijayaraghavan, *Proceedings of the Solid State Physics Symposium* **1991**, *34C*, 126.
[17] J. L. Dormann, C. Godart, M. Latroche, E. Alleno, J. Jove, *Conference Proceedings*, ICAME-95, SIF, Bologna **1996**, *50*, 339.
[18] T. Harmening, W. Hermes, M. Eul, F. M. Schappacher, R. Pöttgen, *Z. Kristallogr.* **2009**, *224*, 351.
[19] M. L. Fornasini, P. Manfrinetti, D. Mazzone, *Z. Kristallogr. NCS* **2003**, *218*, 279.
[20] M. Pani, M. L. Fornasini, P. Manfrinetti, F. Merlo, *Intermetallics* **2011**, *19*, 957.
[21] D. Mazzone, P. L. Paulose, S. K. Dhar, M. L. Fornasini, P. Manfrinetti, *J. Alloys Compd.* **2008**, *453*, 24.
[22] R. Pöttgen, *J. Alloys Compd.* **1996**, *243*, L1.
[23] Z. Hossain, R. Nagarajan, M. Etilé, C. Godart, J. P. Kappler, L. C. Gupta, R. Vijayaraghavan, *J. Magn. Magn. Mater.* **1995**, *150*, 223.
[24] F. Merlo, M. Pani, M. L. Fornasini, *J. Alloys Compd.* **1996**, *232*, 289.
[25] R. Pöttgen, R.-D. Hoffmann, R. Müllmann, B. D. Mosel, G. Kotzyba, *Chem. Eur. J.* **1997**, *3*, 1852.
[26] D. Kußmann, R. Pöttgen, U.Ch. Rodewald, C. Rosenhahn, B. D. Mosel, G. Kotzyba, B. Künnen, *Z. Naturforsch.* **1999**, *54b*, 1155.

[27] F. Merlo, M. Pani, M. L. Fornasini, *J. Less-Common Met.* **1991**, *171*, 329.
[28] R. Pöttgen, *Z. Kristallogr.* **1996**, *211*, 884.
[29] U. Ernet, R. Müllmann, B. D. Mosel, H. Eckert, R. Pöttgen, G. Kotzyba, *J. Mater. Chem.* **1997**, *7*, 255.
[30] S. K. Dhar, P. Paulose, R. Kulkarni, P. Manfrinetti, M. Pani, N. Parodi, *Solid State Commun.* **2009**, *149*, 68.
[31] I. Schellenberg, M. Eul, R. Pöttgen, *Z. Naturforsch.* **2011**, *66b*, 1179.
[32] I. Schellenberg, M. Eul, R. Pöttgen, *Monatsh. Chem.* **2011**, *142*, 875.
[33] I. Schellenberg, U. Pfannenschmidt, M. Eul, C. Schwickert, R. Pöttgen, *Z. Anorg. Allg. Chem.* **2011**, *637*, 1863.
[34] I. Schellenberg, W. Hermes, S. Lidin, R. Pöttgen, *Z. Kristallogr.* **2011**, *226*, 214.
[35] R. Pöttgen, T. Gulden, A. Simon, *GIT Labor-Fachzeitschrift* **1999**, *43*, 133.
[36] D. Kußmann, R.-D. Hoffmann, R. Pöttgen, *Z. Anorg. Allg. Chem.* **1998**, *624*, 1727.
[37] K. Yvon, W. Jeitschko, E. Parthé, *J. Appl. Crystallogr.* **1977**, *10*, 73.
[38] B. Eisenmann, N. May, W. Müller, H. Schäfer, *Z. Naturforsch.* **1972**, *27b*, 1155.
[39] P. Villars, K. Cenzual, Pearson's Crystal Data: Crystal Structure Database for Inorganic Compounds (release 2013/14), ASM International®, Materials Park, Ohio (USA) **2013**.
[40] L. Palatinus, G. Chapuis, *J. Appl. Crystallogr.* **2007**, *40*, 786.
[41] V. Petříček, M. Dušek, L. Palatinus, *Z. Kristallogr.* **2014**, *229*, 345.
[42] R. A. Brand, NORMOS, Mössbauer fitting Program, Universität Duisburg, Duisburg (Germany) **2007**.
[43] J. Nylén, F. J. Garcìa Garcìa, B. D. Mosel, R. Pöttgen, U. Häussermann, *Solid State Sci.* **2004**, *6*, 147.
[44] D. Johrendt, C. Felser, O. Jepsen, O. K. Andersen, A. Mewis, J. Rouxel, *J. Solid State Chem.* **1997**, *130*, 254.
[45] J. Donohue, *The Structures of the Elements,* Wiley, New York **1974**.
[46] A. H. Gomes De Mesquita, K. H. J. Buschow, *Acta Crystallogr.* **1967**, *22*, 497.
[47] R. Pöttgen, *Z. Naturforsch.* **1995**, *50b*, 175.
[48] C. P. Sebastian, L. Zhang, C. Fehse, R.-D. Hoffmann, H. Eckert, R. Pöttgen, *Inorg. Chem.* **2007**, *46*, 771.
[49] R. Pöttgen, P. E. Arpe, C. Felser, D. Kußmann, R. Müllmann, B. D. Mosel, B. Künnen, G. Kotzyba, *J. Solid State Chem.* **1999**, *145*, 668.
[50] R. Pöttgen, *Z. Anorg. Allg. Chem.* **2014**, *640*, 869.
[51] W. Schnelle, J. Engelhardt, E. Gmelin, *Cryogenics* **1999**, *39*, 271.
[52] R.-D. Hoffmann, R. Pöttgen, D. Kußmann, D. Niepmann, H. Trill, B. D. Mosel, *Solid State Sci.* **2002**, *4*, 481.
[53] D. Niepmann, R. Pöttgen, K. M. Poduska, F. J. DiSalvo, H. Trill, B. D. Mosel, *Z. Naturforsch.* **2001**, *56b*, 1.
[54] R. Mishra, R. Pöttgen, R.-D. Hoffmann, H. Trill, B. D. Mosel, H. Piotrowski, M. F. Zumdick, *Z. Naturforsch.* **2001**, *56b*, 589.